Evaluation of Critical Current Density and Residual Resistance Ratio limits in Powder in Tube Nb_3Sn conductors

Christopher Segal[1], Chiara Tarantini[1], Zu Hawn Sung[1], Peter J. Lee[1], Bernd Sailer[2], Manfred Thoener[2], Klaus Schlenga[2], Amalia Ballarino[3], Luca Bottura[3], Bernardo Bordini[3], Christian Scheuerlein[3], David C. Larbalestier[1]

[1]Applied Superconductivity Center, NHMFL, Florida State University, Tallahassee, FL 32310

[2]Bruker EAS GmbH, Ehrichstrasse 10, 63450 Hanau, Germany

[3]CERN, European Organization for Nuclear Research, 1211 Geneva 23, Switzerland

***Abstract*— High critical current density (J_c) Nb_3Sn A15 multifilamentary wires require a large volume fraction of small grain, superconducting A15 phase, as well as Cu stabilizer with high Residual Resistance Ratio (RRR) to provide electromagnetic stabilization and protection. In Powder-in-Tube (PIT) wires the unreacted Nb7.5wt.%Ta outer layer of the tubular filaments acts as a diffusion barrier and protects the interfilamentary Cu stabilizer from Sn contamination. A high RRR requirement generally imposes a restricted A15 reaction heat treatment (HT) to prevent localized full reaction of the filament that could allow Sn to reach the Cu. In this study we investigate recent high quality PIT wires that achieve a J_c(12 T, 4.2 K) up to ~2500 A/mm^2 and find that the minimum diffusion barrier thickness decreases as the filament aspect ratio increases from ~1 in the inner rings of filaments to 1.3 in the outer filament rings. We found that just 2-3 diffusion barrier breaches can degrade RRR from 300 to 150 or less. Using progressive etching of the Cu we also found that the RRR degradation is localized near the external filaments where deformation is highest. Consequently minimizing filament distortion during strand fabrication is important for reducing RRR degradation. The additional challenge of developing the highest possible J_c must be addressed by forming the maximum fraction of high J_c small-grain (SG) A15 and minimizing low J_c large-grain (LG) A15 morphologies. In one wire we found that 15% of the filaments had a significantly enhanced SG/LG A15 ratio and no residual A15 in the core, a feature that opens a path to substantial J_c improvement.**

I. INTRODUCTION

The current impetus to develop Nb_3Sn as an accelerator conductor has been driven by the prospect of upgraded magnet systems for the Large Hadron Collider (LHC) at CERN, where using Nb_3Sn will generate higher magnetic fields in the dipoles and quadrupoles for the High-Luminosity upgrade, as well as for the cable test magnet FRESCA2 [1]. The goal for the LHC Hi-Luminosity conductors is three-fold: to develop fine filament sizes (effective filament diameter, d_{eff}, <50 μm), to maximize the non-Cu J_c (J_c (12 T, 4.2 K) > 2450 A/mm^2), and to assure electromagnetic stability (Residual-Resistance Ratio, RRR, >100) by maintaining the integrity of the diffusion barrier through the cabling process [1]. While each individual requirement has been achieved, a wire which satisfies all three requirements is still challenging**.** We note that the robust and reliable bronze process route [2] of producing Nb_3Sn can only achieve J_c (12 T, 4.2 K) of order 1200 A/mm^2 [3], far too low for accelerator magnets [4],[5]. This leaves PIT and RRP (Rod-Restack Process) wires as the primary candidates for such magnets. They have, to date, reached a maximum J_c(12 T, 4.2 K) of ~2500 A/mm^2 and ~3000 A/mm^2 respectively [1],[6]. While RRP today surpasses PIT in maximum non-Cu J_c at fields of about 12 T, PIT can develop a higher layer J_c of ~6000 A/mm^2, RRP achieving ~5000 A/mm^2 [7].

The PIT method of producing high J_c superconducting wires was first proposed at the Netherlands Energy Research Foundation (ECN) in 1975 by Van Beijnen and Elen who manufactured wires from vanadium tubes filled with powders of V_2Ga_5 or VSi_2 mixed with Cu, where Cu was added to lower the A15 phase formation temperature in the subsequent reaction to form superconducting V_3Ga or V_3Si [8]. The process was soon applied to Nb_3Sn using Nb tubes with $NbSn_2$ and Cu powders [9], and ECN produced wires with up to 180 filaments with A15 layer J_c (12 T, 4.2 K) values of 2200 A/mm^2 (i.e. J_c averaged over the total A15 area within the diffusion barrier) [10]**.** By 1990 a 192 filament Nb_3Sn PIT wire was a standard configuration being manufactured in pre-production quantities with a non-Cu J_c (12 T, 4.2 K) of 1700 A/mm^2[11]. Shape Metal Innovations (SMI) in the Netherlands then took over the process, focusing on two wire architectures: a 36 filament for very high field applications, and a 192 filament for high energy physics (HEP) magnets [12]. Continued optimization of filament size, powder quality, and manufacturing techniques led to a ternary wire of 192 Nb7.5wt%Ta tubes typically containing $NbSn_2$, and Cu powders. After heat treatment (HT), these wires produced volume fractions of each component not too far from what is produced today: 40% small grain (SG) A15, 10% large grain (LG) A15, 25% of residual tube acting as diffusion barrier (DB), and 25% residual core originally filled by $NbSn_2$ and Cu. The non-Cu J_c (12 T, 4.2 K) had advanced to 1780 A/mm^2 [13], the layer J_c growing appreciably to 4280 A/mm^2. These improvements were thoroughly characterized by digital micrograph analysis [14], magnetization [15], and strain dependence [16] among other techniques summarized in [17].

In 2006 European Advanced Superconductor (now: Bruker EAS) acquired the PIT technology from SMI; in addition to increasing production to industrial scale, they also improved the design in two significant ways: one by switching from hexagonal to round filaments (which allows the radial A15 reaction to use the Nb(Ta) tube more efficiently) , and two by reducing the filament diameter, which resulted in increasing the non-Cu J_c (12 T, 4.2 K) to 2500 A/mm^2 [18]. However, it appears that a major obstacle to further increasing J_c is the presence of a large grain A15 layer between the Sn source of the core and the desired high J_c SG A15 layer. As we have recently shown elsewhere, this LG layer has a high T_c but it does not contribute to the transport current density [19], thus degrading the efficiency of the non-Cu package. This is partially due to a poor superconducting pathway imposed by Cu precipitated between the large grains of A15, and partly due to it not having the small (diameters ~100 nm or less) grain size desired for strong vortex pinning [20]. Because the LG A15 fraction is about a quarter of the total A15 in PIT, a significant part of the J_c difference between PIT and RRP lies here [21], [7].

An additional obstacle to high non-Cu J_c is that the amount of residual diffusion barrier needed to maintain high RRR for PIT is greater than in RRP. In a recent detailed evaluation of a 54/61 Nb7.5wt%Ta RRP conductor by Tarantini *et al*., a J_c(12 T, 4.2 K) of 3000 A/mm^2 was obtained in a wire whose subelements are made of ~60% A15, a protective residual DB of ~7%, and a residual core of 33% [7]. RRP designs, however, have recently evolved to a greater number of sub-elements (108 to 150) and with the finer filament size, the DB fraction increases to ~10% and the J_c drops to ~2750 A/mm^2, diminishing the differences between PIT and RRP.

The purpose of this work is to provide a similarly detailed analysis of three different billets of 192 filament PIT wires recently manufactured by Bruker EAS for use at CERN [22]. We want to understand the nature of the A15, DB and residual core phase fractions and to relate these to the RRR and J_c values in support of the great interest of the HEP community ([23], [24]) in developing high J_c magnet conductors, as well as fundamental studies of the quality of the A15 phase [25]. We also wanted to compare our evaluations of these recent conductors with those that we made on earlier SMI-made variants of PIT reported in [13], [18], [26].

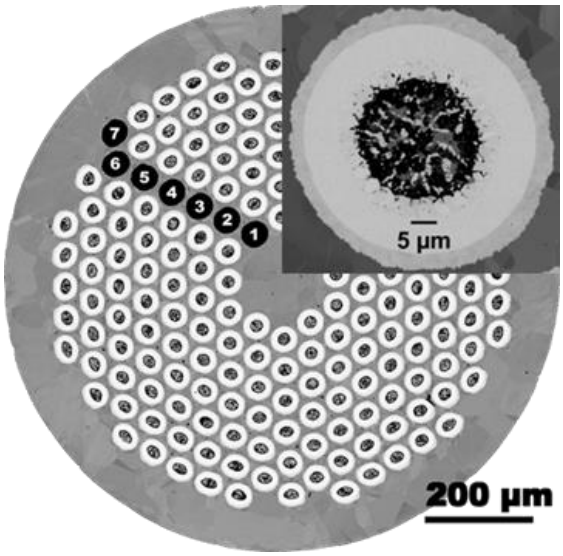

Figure 1: FESEM-BSE images of polished, transverse cross-sections of a reacted Bruker PIT wire 1mm in diameter with 192 superconducting filaments organized into 7 rings within a matrix of stabilizing Cu. Inset image is of a typical filament from inner ring 1.

II. EXPERIMENTAL DETAILS

The PIT wires analyzed here were manufactured by Bruker EAS using 192 Nb7.5wt%Ta tubes containing mostly $NbSn_2$, Nb, and Cu powders in a solid Cu stabilizer matrix (as seen after reaction in **figure 1**). To produce the multifilamentary wire, 192 such monofilaments are drawn, cut, stacked into a multifilament form, and then processed down to wire diameters between 1.25 and 0.7 mm. Upon heat treatment the reaction proceeds by Sn diffusing radially outward into the Nb(Ta) tube wall from the nominally circular Sn-rich cores (the residual unreacted tube is effectively the diffusion barrier). A typical cross-section is shown in **figure 1**. The 192 superconducting filaments are arranged in 7 concentric rings, which we number from the inside (ring 1) to outside (ring 7) and they are set in a stabilizing Cu matrix. Geometric distortion of the filaments during fabrication of the strand leads to variation in the residual thickness of the diffusion barrier during reaction, opening up the possibility of Sn leaking into the Cu if the A15 front locally reacts through the DB. After the reaction, the non-Cu area is composed of a residual Nb-7.5wt.%Ta diffusion barrier, a superconducting layer with both large grain (LG) and small grain (SG) A15, and a remnant core containing various intermetallics, as well as some disconnected A15 grains and voids. The two requirements for an optimized heat treatment which we focus on here are that RRR should not degrade below 150 and that $J_c(12\,\mathrm{T}, 4.2\,\mathrm{K})$ should exceed 2450 A/mm^2. Here RRR is given by the ratio $\rho(300\,\mathrm{K})/\rho(19\,\mathrm{K})$. Throughout this paper samples will be identified by their final heat treatment (HT) temperature and time, (e.g. 625°C for 280 hours is 625/280) and their wire diameter. The tight constraints on high J_c *and* high RRR meant that heat treatments varied only from 620-670°C for 50-240h **[table I]**.

Table I: Parameters of the three wires studied, filament diameter is of reacted wires

Wire Diameter (mm)	Heat Treatment			filament diamter (µm)
	Temp (?C)	Time (h)	RRR	
1.0	620+640	120+120	175	50
1.0	625	280	166	50
0.85	630	100	299	42
0.85	630	200	161	42
0.85	650	50	291	42
0.85	650	100	177	42
0.85	670	50	130	42
0.85	670	100	67	42
0.78	630	240	49	39
0.78	630	240	49	39

Digital Imaging was performed using a Zeiss 1540 Crossbeam® Field Emission Scanning Electron Microscope (FESEM) coupled with digital analysis software to allow rapid and accurate evaluation of the positional variation, and geometric distortion of each filament ring by ring. The backscattered electron (BSE) intensity in the FESEM is sensitive to atomic number (Z) and phases with a higher effective Z are brighter in the BSE image, as seen in **figure 1**. These data combined with knowledge of what phases exist in the sample allow quick identification of the Cu,

Nb-7.5wt.%Ta, and $Nb(Ta)_3Sn$ layers. With these techniques we can isolate the unreacted DB annulus and from this measure the DB thickness separating the A15 layer and the Cu. We can also measure the area fractions of each phase with the widely used open-source software package, Fiji [27] (based on ImageJ [28]), allowing us to make high precision comparisons between samples.

In addition, the occurrence of barrier breakthrough is quantified (where the residual Nb-Ta layer thickness goes to zero and the A15 phase is in direct contact with the Cu stabilizer). We then determined the local impact of barrier breakthrough on RRR by progressively etching away the matrix Cu and re-measuring the RRR at intervals. Resistivity measurements were made in a Physical Property Measurement System (PPMS) by attaching four-point contacts with silver epoxy. After each measurement the silver epoxy was removed and the sample immersed in a dilute nitric acid bath for 5-10 minutes to partially remove the Cu matrix. The RRR was then measured again, repeating this etch and measurement process until only ~4-5 inner rings of filaments remained. Transverse cross-sections showing the approximate depths of each etch are shown in **figure 2**.

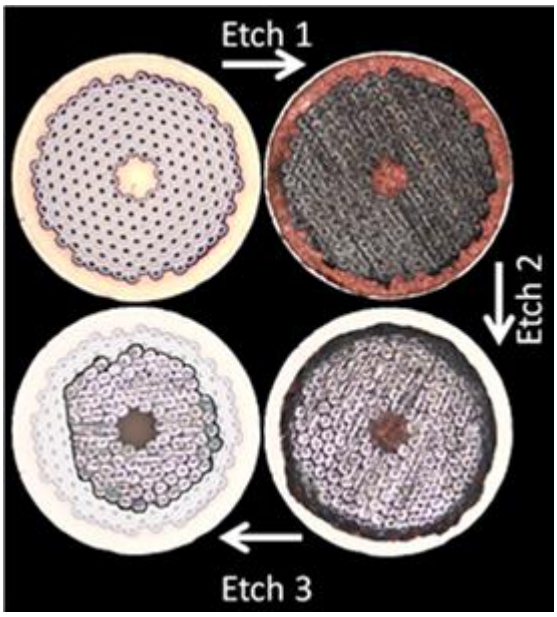

Figure 2: Light microscope images of a progressively etched 1 mm-diameter PIT wire. The images of the etched wire are overlaid on the initial cross section. Top left is the initial wire, moving clockwise the wire after a small annulus of outer Cu was removed in etch 1, and after most external Cu was removed and the filament pack revealed (etch 2). Etch 3 removed the outer two filament rings, as well as some interfilamentary Cu further into the wire. RRR was measured after each etch as is shown in figure 7.

III. RESULTS

1) Filament Deformation and Barrier Failure Effect

If the filaments have a circular cross-section they will have an aspect ratio of 1, however, mechanical processing to final size results in some distortion of the filaments, especially in the outer rings. We can classify the resulting filaments into three distinct types: the majority of filaments retain their round shape with little distortion as seen in **figure 3a**, however about 15% are aspected beyond 1.15 with substantial thinning of the DB on the side facing the wire center, and a thickening of the outer side **[fig 3b]**. Within this 15%, we typically see two to three filaments with barrier breakthrough as shown in **figure 3c**, where the A15 reaction front is in direct contact with the Cu layer.

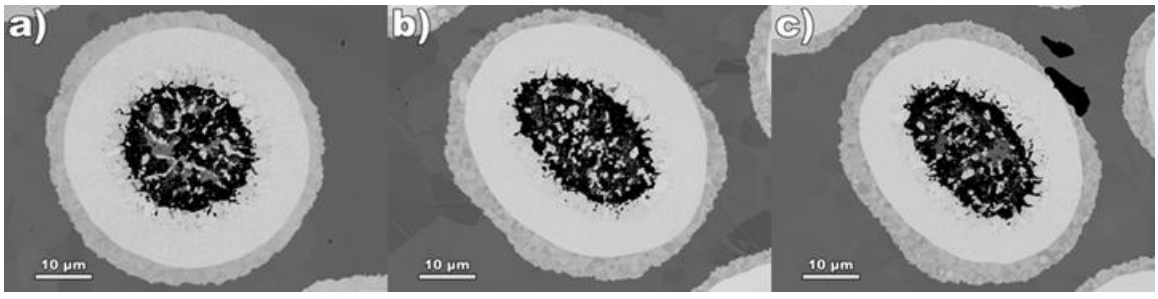

Figure 3: FESEM-BSE images of polished, transverse cross-sections of representative filaments from the 1 mm diameter conductor after reaction of 120 h at 620 °C + 120 h at 640 °C. Each image is oriented with the wire center towards the upper right. a) Typical inner ring filament with aspect ratio close to 1 and rather uniform residual diffusion barrier thickness. b) Typical outer ring filament with aspect ratio ~ 1.3 showing barrier thinning on the side facing the wire center. c) A broken outer ring filament where the A15 layer touches the Cu at top right and allows Sn leakage into the Cu and degradation of RRR. Despite the leakage however, this sample still maintained RRR = 175.

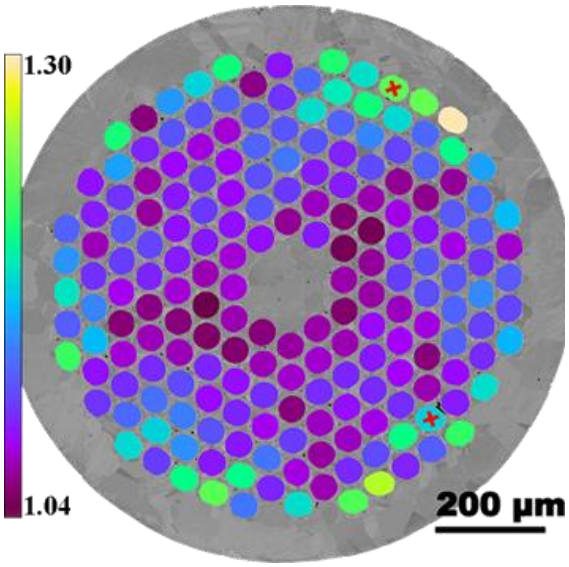

Figure 4: Color-coded representation of filament aspect ratio showing a range from 1.04 (dark/purple) to 1.30 (light/tan). The two filaments with barrier breakthrough are marked with a red x. This 1 mm diameter wire was reacted for 120 h at 620 °C + 120 h at 640 °C and had RRR= 175.

Severe DB breakdowns can often be found by the appearance of Kirkendall voids in the surrounding Cu [29].In **figure 4** the whole cross-section is color-coded to show variation in the aspect ratio which increases from a minimum of 1.04 in ring one up to a maximum of 1.30 in ring seven. The two or three broken barriers occur in the more distorted filaments of the outer two rings. However, it should be noted that the Sn which is lost to the Cu in broken filaments typically has little impact on A15 production since barrier breakthrough occurs towards the end of the reaction. However, when the leak is large it forms a Kirkendall void, the A15 area can be reduced by more than 10%. **Figure 5** shows that when the Sn does leak into the Cu, it can form A15 phase on the *outside* of the diffusion barrier. In **figure 5b** we see a leak in ring seven that was large enough to form a Kirkendall void nearly 20 µm wide between the A15 and the stabilizing Cu. The A15 has formed not only on the outside of the broken filament, but also on the neighboring filament, thus demonstrating the significant mobility of Sn in Cu. Figures **5d and 5e** show that this external A15 forms as far in as ring four, despite breaks generally occurring only in the outer two rings (6 and 7). We then measured the variation in barrier thickness around each filament, separating the results by ring number in **figure 6**, and found that the distortion is relatively constant for the inner rings (1-4), but increases linearly from ring 5 to 7. Although the mean barrier thickness varies by less than 5% for all rings, the standard deviation grows substantially in the outer rings. For rings one through four there is little variation of minimum thickness (0.8-1.1 µm), maximum thickness (4.6-5.1 µm), or standard deviation (0.6-0.7 µm). However, in rings 5 to 7, the maximum thickness gets as high as 7 µm, while the minimum goes to zero due to the A15 reaction front reaching the Cu (**figure 3c)**. Most noticeable is the widening of the distributions, the standard deviation of outer filament rings almost doubling to 1.3 µm compared to the inner rings. Although only two or three filaments actually leaked, breakdown is imminent in multiple filaments due to the stronger local distortions in the outer rings, even with the barriers globally comprising ~25% of the non-Cu area. These signs of incipient DB failure are of definite concern when considering the additional filament distortion occurring during the Rutherford cable manufacture, particularly at narrow cable edges [30]. Resistance measurements of wires with 2-3 (out of the 192) broken barriers have RRR values ranging from 130-175. To directly characterize the impact of barrier breakthrough on the surrounding Cu stabilizer, an experiment was designed to investigate local RRR (as seen in **figure 2**). Progressive Cu etching of the 1 mm wires as shown in **figure 7** reveals that RRR steadily degrades from 166-175 to 93-125 with removal of the outer sheath of Cu until the filament pack is exposed. Removing the two outer filament rings containing the 2 or 3 broken barriers and their surrounding degraded Cu shows RRR returning to >170.

2) Heat Treatment Effects on Microstructure and Electrical Properties

To determine how the A15 grain morphology changes with HT time and temperature, we analyzed 0.85 mm wires from six different heat treatments, quantifying the fractions of residual Nb-Ta barrier, small and large grain A15, and remnant core in each case, as is summarized in **table II**. **Figure 8** contrasts filament images from the least and most reacted samples. At the lower temperature HT of 630/100 we see a large amount of remnant DB (35%) and isolated A15 in the core (5%). The higher temperature HT at 670/100 shows the core nearly depleted of A15, less residual DB (22%), and a larger amount of both SG (44%) and LG A15 (15%).

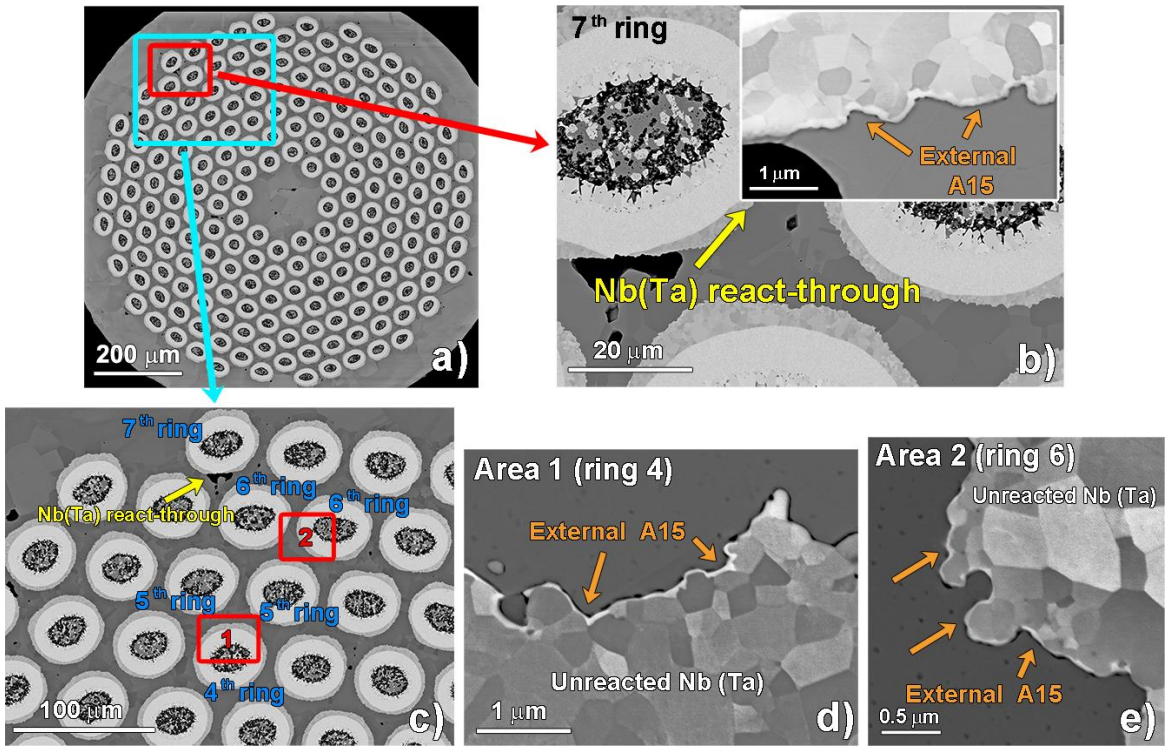

Figure 5: FESEM-BSE images of polished, transverse cross-sections of a PIT wire. a) Whole wire overview, b) Close up of A15 formation external to a breached diffusion barrier in outer ring 7 and a Kirkendall void formed by dissolution of Sn in the stabilizing Cu, c) Overview of filaments in rings 3-7 in the vicinity of the breach, d, e) A15 formation on barrier outsides appears as far away as ring four. This 1 mm diameter wire was reacted for 280 h at 625 °C and RRR = 166.

The average large grain (> 1 μm diameter) A15 volume fraction is ~15% (all % referred to the non-Cu cross-section) and, while slightly higher for the 670/100, the amount varies little with HT, as its Nb_6Sn_5 precursor is created early in the reaction by decomposition of the Cu-Nb-Sn intermetallic phase typically identified in the literature as "Nausite". This Sn-rich reaction pathway tends to follow $NbSn_2$ + Cu → Cu-Nb-Sn (Nausite) → $NbSn_2$ →Nb_6Sn_5→ LG Nb_3Sn [31], [32].

The residual core cross-section after reaction is made of 18 to 20% ternary phases or voids, and up to 5% disconnected A15. There is a clear trend that higher reaction temperatures decrease the amount of A15 in the core. The SG A15(< 1 μm diameter, typically 100-200 nm) varies from 28 to 44%. As the diffusion barrier is consumed to produce SG A15, its volume fraction decreases from 35 to as little as 22%.

The data in **figure 9** shows the relationship between the non-Cu J_c and RRR for the 0.85 mm and 1 mm wires. It shows two groups of data for these eight samples. The two lowest J_c samples (1800 A/mm^2) went through restricted HT's of 630/100 and 650/50. They show a very high RRR of near 300, but only 28% and 30% small grain A15 respectively, significantly less than optimum wires. Wires with the higher J_c (12 T, 4.2 K) values of ~2400 A/mm^2 have RRR <175 and show ~40% small-grained A15.

In the 0.78 mm wire heat treated at 630/240, we found two distinct filament types; ~85% of filaments have the typical microstructure shown in **figure 10a**, which is similar to all other wires in **table II** with J_c > 2300 A/mm^2. However, the other ~15% of filaments have a remarkably different microstructure with significantly different volume fractions of every phase, also including a Cu-rich phase surrounding the LG A15 on the core side as seen in **figure 10b and 10c**. In these atypical filaments, the highly desirable SG A15 layer is enhanced from 41% to 46%, and the LG A15 is suppressed from 14% to 10%, with no A15 remaining in the core. However, we also observe a greater consumption of the DB which drops from 23% to 18%.

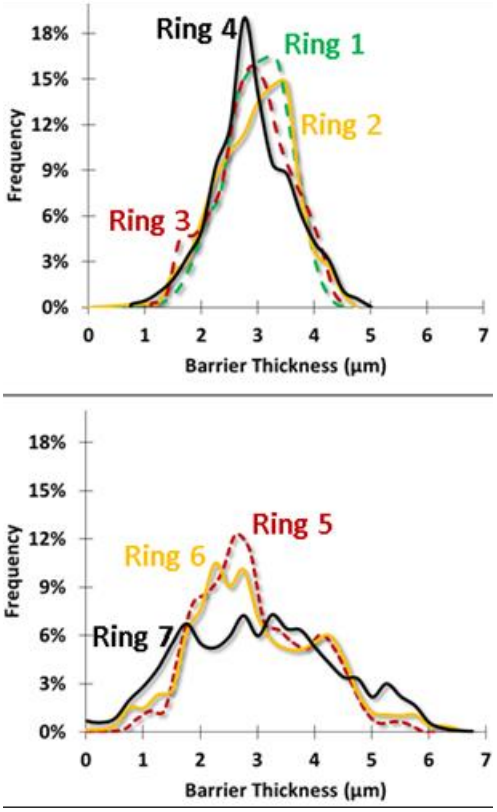

Figure 7: Distribution of residual barrier thicknesses within each of the seven rings of filaments in a 1 mm wire after reaction of 280 h for 625˚C. Distortion is small in the four inner rings but significantly worsens in outer rings five to seven.

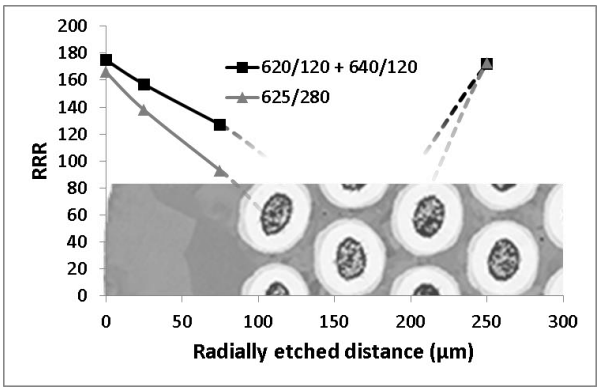

Figure 6: RRR values as measured after each step of the progressive Cu etch, with inlay showing to what depth the Cu was removed before RRR measurement. Dashed lines are shown to guide the eye, and indicate the likely RRR profile in the filament pack based on our analysis of where filaments break

IV. Discussion

From analysis of the reaction products in the non-Cu region, J_c measurements, and RRR, it is convenient to group the wires in **Table 1** into three categories: under-reacted, optimally reacted, and over reacted. The 630/100 And 650/50 wires fall into the under-reacted group: they show significantly less small grain A15 (28-30%), low J_c (12 T, 4.2 K)~1800 A/mm^2, and a high RRR of order 300 that is almost undiminished from the pre-reacted state. Optimally reacted wires are characterized by achieving a near maximum J_c (12 T, 4.2 K) of 2400-2500 A/mm^2 without RRR falling below 150. Such reactions greatly raise J_c at least partially by raising the SG A15 fraction from 28-30 to 40-42%. Over-reaction raises the SG fraction only marginally to about 44% without producing any significant increase in J_c , however, it reduces the RRR to the 50-70 range. This terminal extent to the reacted layer develops a maximum Nb_3Sn content around 59%, of which we believe only the 3/4 made of SG A15 carries useful transport current [18]. It is clear from **Figure 7** that to ensure an adequately high RRR, thinning of the DB must be avoided by limiting the reaction. It can also be seen from **Table II** that the core volume (remnants + core A15) ranges from 22-24% in the lightly reacted state to 19-20% in the most highly reacted state. By contrast there are much bigger changes in the residual DB, which can fall to as little as 22% in the 670/100 HT. Prior to reaction, the proportions of DB and core were 68% and 32% respectively.

The morphological variation of the A15 phase in the filaments is also of strong interest, since it is very clear from many studies that high J_c (12 T) can only be obtained if the A15 grain size (diameter) is held to less than ~150 nm [4], [20]. Moreover, the fraction of the non-Cu package converting to A15 is also important, especially because this appears to be somewhat lower in PIT conductors than in RRP conductors when RRR is kept >150. PIT wires with effective filament diameter under 50 μm show ~57% of total A15, as opposed to ~59% in a recent study of RRP, albeit with a larger effective filament diameter of 70 μm [7]. In addition, the diffusion barrier is the principal Nb source to produce Nb_3Sn in PIT, so there is always a risk of reacting through in making the A15. Furthermore, as the reaction proceeds radially outwards from the core through the filament, both of which inevitably having some degree of distortion (especially after cabling), there needs to be a significant amount of unreacted tube

left for safety. In RRP conductors the diffusion barrier lies outside the Cu matrix in which the Nb filaments are encased and is thus less reacted than the Nb filaments used to form the majority of Nb_3Sn. It should be noted that reacting for longer times without regard to RRR can increase the A15 (almost all SG) to 66% in RRP [7], while PIT does not see any appreciable A15 layer growth beyond the terminal limit.

Table II: Microstructural characterizations and physical properties of interest as described in the text.

HT	wire diameter (mm)	RRR	J_c non-Cu (12T, A/mm^2)	layer J_c (12T, A/mm^2)	vol. %					
					DB	A15 total	remnant	A15 core	A15 LG	A15 SG
620/120+640/120	1.0	175	2500	6158	23.0%	57.9%	19.1%	3.0%	14.2%	40.7%
625/280	1.0	166	2450	6171	23.6%	57.7%	18.7%	3.5%	14.5%	39.7%
630/100	0.85	299	1830	6536	34.5%	46.4%	19.1%	5.1%	13.3%	28.0%
630/200	0.85	161	2380	6280	24.9%	55.4%	19.7%	3.0%	14.5%	37.9%
650/50	0.85	291	1779	5910	32.8%	48.3%	18.9%	2.8%	15.4%	30.1%
650/100	0.85	177	2367	5992	24.6%	57.2%	18.2%	1.3%	16.4%	39.5%
670/50	0.85	130	2404	5683	24.4%	57.0%	18.6%	1.0%	13.7%	42.3%
670/100	0.85	67	2433	5580	22.2%	59.4%	18.4%	0.6%	15.2%	43.6%
630/240(typical)	0.78	49	-	-	22.7%	58.1%	19.2%	3.0%	14.4%	40.7%
630/240(atypical)	0.78	49	-	-	18.2%	56.5%	25.3%	0.0%	10.2%	46.3%
unreacted	0.78	294	-	-	68%	-	32%	-	-	-

There is another important issue separating PIT and RRP conductors that must also be treated explicitly, that is the three distinct A15 grain morphologies found in these high J_c conductors: small grain (<200 nm), large grain (>1 μm), and core grains. The most ineffective for raising the transport J_c is the up to 5% A15 found in the core

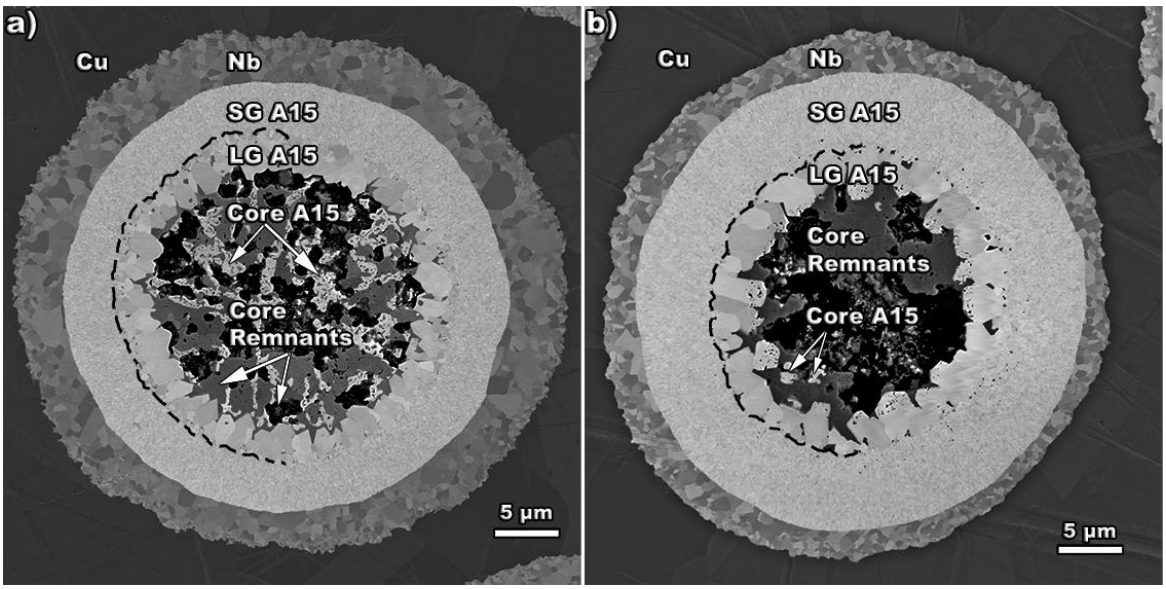

Figure 8: FESEM-BSE images of polished, transverse cross-sections of minimally distorted inner ring filaments of the 0.85 mm wire at the two extreme HTs studied: a) 630 ˚C for 100 h and b) 670 ˚C for 100 h. Crystallographic orientation contrast reveals the small and large grain A15 layers. A dashed line has also been added to better illustrate the interface between the two A15 regions.

(Table II) because it is completely disconnected. It also retains Sn that could otherwise be utilized by the rest of the non-Cu package to produce small, connected A15 grains. Surrounding the core is an annulus of large grain A15, about 20-25% of the total A15. It does not have the SG morphology needed for strong vortex pinning. Recent studies of the magnetization and specific heat by Tarantini *et al.* [19] have shown that most of these grains are poorly connected electromagnetically, and are unable to carry any high-field transport current. Although the mechanism of formation of the LG is still under investigation, Ta was detected in the LG layer by EDS, suggesting that at least part of it forms by the reaction with the tube, consistent with the results of [19] that the LG are in dirty limit. In RRP conductors there are very few LG and they are difficult to quantify as the largest grains typically do not exceed 1 μm [7]. The greater volume fraction of SG A15 in RRP is undoubtedly one reason why the maximum values of J_c (12 T, 4.2 K) in RRP conductors fall in the 2800-3000 A/mm^2 range.

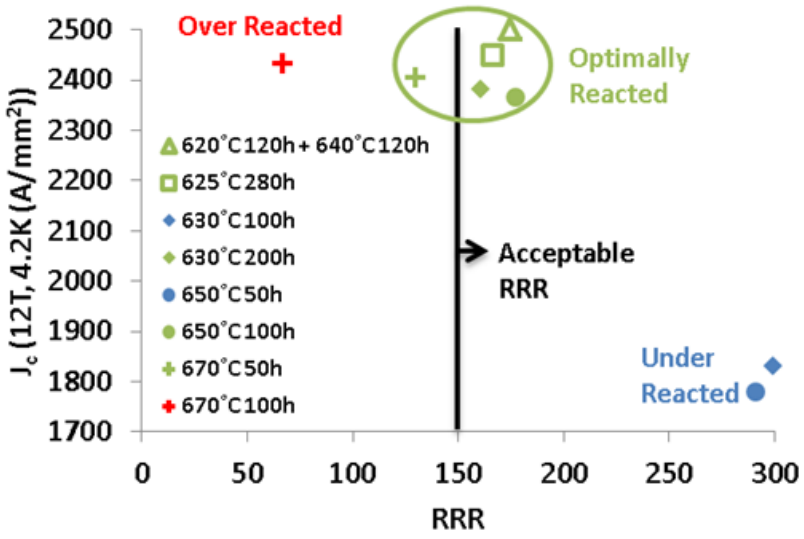

Figure 9: Correlation plot of Jc (12 T, 4.2 K) and RRR for 1mm and 0.85 mm PIT wires. The data show a high Jc cluster with lower RRR and a low J_c cluster with high RRR > 250. Green points indicate optimally reacted wires, blue and red points indicating under reacted and over reacted wires. The 1 mm wires are marked with open symbols and have slightly higher J_c than the 0.85 mm wires.

In these 192 filament conductors, the non-Cu J_c (12 T, 4.2 K) has a clear upper limit of ~2500 A/mm^2. However, it is also important to consider the quality of this SG layer since the effective vortex pinning of the grain boundaries can vary significantly depending on the A15 composition [4]. As we argue above and in reference 18, we can assume that only the SG A15 carries significant transport current and thus we can derive a SG layer J_c by normalizing the non-Cu J_c to the SG layer. In **table II** there is a notable decrease in this layer J_c as the heat treatment temperature increases, consistent with the SG A15 grain growth and decreased GB density at higher reaction temperatures. In general, more A15 can be produced by reacting longer or at higher temperatures, but the present results show that producing more A15 in this manner neither benefits the A15 layer nor the non-Cu J_c values, while also leading to unacceptable RRR degradation. These factors are what constrain reactions into a narrow window at lower temperature where RRR can be maintained in this billet design. Although a thin Ta sleeve on the outside of the NbTa tube might prevent Sn-poisoning of the Cu stabilizer [33] , this approach adds significant additional complexity to the conductor, not least for additional cost and concern about the very different work-hardening characteristics of Nb and Ta.

Close examination of the 0.78 mm wire 630/240 produced an interesting result, however. As shown in **Figure 10,** a small fraction (~15%) of distinctly atypical filaments with substantially different microstructures was found in one cross-section and it suggests that the present reaction box is not a rigid one. In these atypical filaments up to 46% SG A15 was found, despite the relatively low reaction temperature. By contrast the more typical 85% of filaments (typical also of the other two wires) generated the more usual 41% SG A15. The LG A15 amounts of the typical and atypical were 14% and 10% respectively, thus suggesting that J_c might be increased by about 15% if the atypical microstructure could be developed throughout. The core A15 was also entirely suppressed in atypical filaments. Considering the reduction of the LG area, the absence of A15 in the core and reduced residual DB, it is clear the Sn is utilized much more efficiently in these atypical filaments. However, this smaller diameter wire also

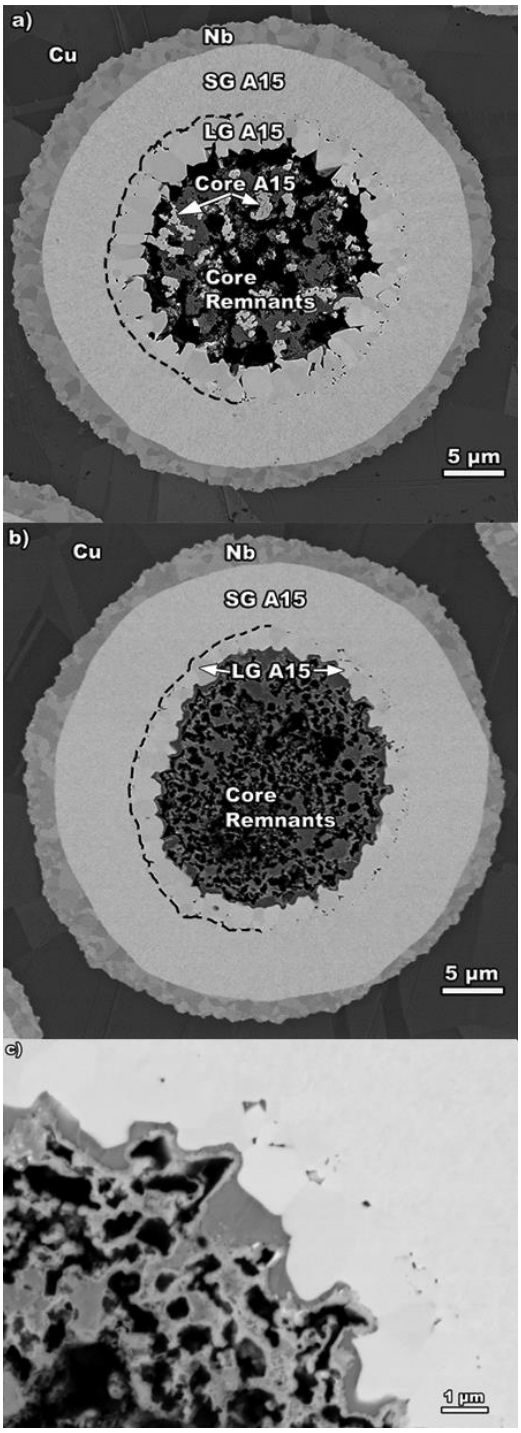

Figure 10: FESEM-BSE images of polished, transverse cross-sections of filaments in a 0.78 mm wire heat treated at 630°C for 240 hours, showing typical (a), and atypical (b) microstructures. The atypical filament has no core A15, a diminished large grain A15 fraction and an enhanced small grain A15 fraction. An artificial dashed line has been added to better distinguish regions of small and large grain A15 morphologies. In addition, there is the appearance of a Cu rich membrane (c) which separates the LG A15 annulus from the core remnants

exhibited a lower RRR of 49 both before and after the reaction, abnormally low considering that the under-reacted RRR of the 0.85 mm wires was near 300, and because all barriers appeared intact after reaction. A low RRR value was also found using the Bruker recommended HT(620/100+640/90) [34]. Subsequent analysis of other cross-sections from the same length did not show these atypical filaments leading us to conclude that their formation was an end-effect in this particular sample associated with local heating during welding of the sample ends prior to reaction heat treatment. Typically, wires are prepared by crimping the end to seal them, and short lengths <1cm are cut from the center of the wire for metallographic analysis, thereby avoiding any end effects. Nevertheless, it is interesting to speculate what J_c properties a completely atypical wire might develop if the effects of this local temperature excursion could be replicated along the entire length of the strand. Assuming that the 0.78 mm wire with all *typical* filaments reaches ~2500 A/mm^2 with a layer J_c of ~5900 A/mm^2, we could then enhance the non-Cu J_c by the ratio of the SG fractions (0.463/0.407 = 1.14) suggesting a J_c (12 T, 4.2 K) of 2500 x 1.14 = 2840 A/mm^2. This enhanced J_c would be a significant step along the way to the desired accelerator strand properties [6].

V. CONCLUSION

Our quantitative image analysis of reacted PIT conductors shows that the outer filament rings tend to contain more distorted filaments than inner rings which results in diffusion barriers that are thinner on the side facing the wire center, making barrier breakthrough more likely in outer rings. It should be noted, however, that a study of PIT wires rolled to simulate cabling damage [34] shows that this damage tends to occur mostly to the inner filament rings, thus the filament quality of all rings is important. It is well known that once the A15 reacts through the diffusion barrier, Sn can diffuse into the Cu stabilizer and the local RRR is degraded and electromagnetic stability compromised, and in this study we show how this RRR degradation is localized to the rings where the most react-throughs occur.

We show that of the A15 formed during reaction, only about 3/4 is small grain and current carrying, the rest being large grain A15 of poor connectivity. J_c (12 T, 4.2 K) saturates at around 2500 A/mm^2 even when longer or hotter reactions can produce more A15.

Thus the current filament design represents a necessary compromise between maximizing the A15 layer thickness and maintaining RRR.

Atypical filaments were found in one cross-section that showed a higher fraction of small grain A15 which we believe was due to a local temperature excursion during wire end sealing prior to heat treatment, leading us to believe that there may still be opportunities to modify the heat treatments or core content to produce a better large grain to small grain ratio. A broader range of HT evaluations are underway, which will include studying the effects of multi-step heat treatments, with a view to finding the limits to reaction for this wire design which is very promising as a high J_c, fine filament conductor for high field magnet use.

VI. Acknowledgements

This work was supported by the US Department of Energy (DOE) Office of High Energy Physics (award DE-SC0012083 and DE-FG02-07ER41451), by CERN (contracts KE1920 and KN2713), by the National High Magnetic Field Laboratory (which is supported by the National Science Foundation under NSF/DMR-1157490) and by the State of Florida. The PIT strand was supplied to us by the US LHC Accelerator Research Program (LARP), which is a BNL, FNAL, LBNL, and SLAC collaboration with CERN for the High Luminosity LHC program: http://www.uslarp.org/

Frequent discussions with C. Sanabria and M. Brown at ASC-FSU are greatly acknowledged.

VII. References

[1] L. Bottura, G. de Rijk, L. Rossi, and E. Todesco, "Advanced Accelerator Magnets for Upgrading the LHC," *IEEE Trans. Appl. Supercond.*, vol. 22, no. 3, pp. 4002008–4002008, Jun. 2012.

[2] D. C. Larbalestier, P. Madsen, J. Lee, M. Wilson, and J. Charlesworth, "Multifilamentary niobium tin magnet conductors," *IEEE Trans. Magn.*, vol. 11, no. 2, pp. 247–250, Mar. 1975.

[3] Y. Murakami, H. Kato, H. Kurahashi, and T. Miyatake, "Improvement in Characteristics of Bronze-processed Nb_3Sn Superconducting Wires," *TEION KOGAKU J. Cryog. Supercond. Soc. Jpn.*, vol. 47, no. 8, pp. 474–478, 2012.

[4] P. J. Lee and D. C. Larbalestier, "Microstructural factors important for the development of high critical current density Nb_3Sn strand," *Cryogenics*, vol. 48, no. 7–8, pp. 283–292, Jul. 2008.

[5] A. Ballarino and L. Bottura, "Targets for R&D on Nb_3Sn Conductor for High Energy Physics," *IEEE Trans. Appl. Supercond.*, vol. 25, no. 3, pp. 1–6, Jun. 2015.

[6] M. B. Field, Y. Zhang, H. Miao, M. Gerace, and J. A. Parrell, "Optimizing Conductors for High Field Applications," *IEEE Trans. Appl. Supercond.*, vol. 24, no. 3, pp. 1–5, Jun. 2014.

[7] C. Tarantini, P. J. Lee, N. Craig, A. Ghosh, and D. C. Larbalestier, "Examination of the trade-off between intrinsic and extrinsic properties in the optimization of a modern internal tin Nb_3Sn conductor," *Supercond. Sci. Technol.*, vol. 27, no. 6, p. 065013, Jun. 2014.

[8] C. van Beijnen and J. Elen, "Potential fabrication method of superconducting multifilament wires of the A-15 type," *IEEE Trans. Magn.*, vol. 11, no. 2, pp. 243–246, Mar. 1975.

[9] J. Elen, C. van Beijnen, and C. van der Klein, "Multifilament V_3Ga and Nb_3Sn superconductors produced by the ECN-technique," *IEEE Trans. Magn.*, vol. 13, no. 1, pp. 470–473, Jan. 1977.

[10] C. van Beijnen and J. Elen, "Multifilament Nb_3Sn superconductors produced by the E.C.N. technique," *IEEE Trans. Magn.*, vol. 15, no. 1, pp. 87–90, Jan. 1979.

[11] E. M. Hornsveld and J. D. Elen, "Development of Niobium-Tin Conductors at ECN," *Adv. Cryog. Eng.*, vol. 36A, pp. 157–160, 1990.

[12] J. L. H. Lindenhovius, E. M. Hornsveld, A. den Ouden, W. A. J. Wessel, and H. H. J. ten Kate, "Progress in the development of Nb_3Sn conductors based on the 'Powder in tube' method with finer filaments," *IEEE Trans. Appl. Supercond.*, vol. 9, no. 2, pp. 1451–1454, Jun. 1999.

[13] C. M. Fischer, "Investigation of the Relationships Between Superconducting Properties and Nb_3Sn Reaction Conditions In Powder-In-Tube Nb_3Sn Conductors," University of Wisconsin - Madison, 2002.

[14] C. M. Fischer, P. J. Lee, and D. C. Larbalestier, "Irreversibility field and critical current density as a function of heat treatment time and temperature for a pure niobium powder-in-tube Nb_3Sn conductor," in *AIP Conference Proceedings*, 2002, vol. 614, pp. 1008–1015.

[15] A. Godeke, M. C. Jewell, C. M. Fischer, A. A. Squitieri, P. J. Lee, and D. C. Larbalestier, "The upper critical field of filamentary Nb_3Sn conductors," *J. Appl. Phys.*, vol. 97, no. 9, p. 093909, Apr. 2005.

[16] B. ten Haken, A. Godeke, and H. H. J. ten Kate, "The strain dependence of the critical properties of Nb_3Sn conductors," *J. Appl. Phys.*, vol. 85, no. 6, pp. 3247–3253, Mar. 1999.
[17] A. Godeke, "A review of the properties of Nb_3Sn and their variation with A15 composition, morphology and strain state," *Supercond. Sci. Technol.*, vol. 19, no. 8, p. R68, Aug. 2006.
[18] C. D. Hawes, "Investigations of the Inhomogeneity of a Powder-In-Tube Nb_3Sn Conductor," University of Wisconsin - Madison, 2000.
[19] C. Tarantini, C. Segal, Z. H. Sung, P. J. Lee, L. Oberli, A. Ballarino, L. Bottura, and D. C. Larbalestier, "Composition and connectivity variability of the A15 phase in PIT Nb_3Sn wires," *Supercond. Sci. Technol.*, vol. 28, no. 9, p. 095001, Sep. 2015.
[20] R. M. Scanlan, W. A. Fietz, and E. F. Koch, "Flux pinning centers in superconducting Nb_3Sn," *J. Appl. Phys.*, vol. 46, no. 5, pp. 2244–2249, May 1975.
[21] J. A. Parrell, Y. Zhang, M. B. Field, P. Cisek, and S. Hong, "High field Nb_3Sn conductor development at Oxford Superconducting Technology," *IEEE Trans. Appl. Supercond.*, vol. 13, no. 2, pp. 3470–3473, Jun. 2003.
[22] L. B. B Bordini, "Extensive Characterization of the 1 mm PIT Nb_3Sn strand for the 13-T FRESCA2 Magnet," *IEEE Trans. Appl. Supercond.*, vol. 22, no. 3, 2012.
[23] S. A. Gourlay, G. Ambrosio, N. Andreev, M. Anerella, E. Barzi, R. Bossert, S. Caspi, D. R. Dietderich, P. Ferracin, R. Gupta, A. Ghosh, A. R. Hafalia, C. R. Hannaford, M. Harrison, V. S. Kashikhin, V. V. Kashikhin, A. F. Lietzke, S. Mattafirri, A. D. McInturff, F. Nobrega, I. Novitsky, G. L. Sabbi, J. Schmazle, R. Stanek, D. Turrioni, P. Wanderer, R. Yamada, and A. V. Zlobin, "Magnet R&D for the US LHC Accelerator Research Program (LARP)," *IEEE Trans. Appl. Supercond.*, vol. 16, no. 2, pp. 324–327, Jun. 2006.
[24] D. R. Dietderich and A. Godeke, "Nb_3Sn research and development in the USA – Wires and cables," *Cryogenics*, vol. 48, no. 7–8, pp. 331–340, Jul. 2008.
[25] C. Senatore and R. Flukiger, "Formation and upper critical fields of the two distinct A15 phases in the subelements of powder-in-tube Nb_3Sn wires," *Appl. Phys. Lett.*, vol. 102, no. 1, pp. 012601–012601–4, Jan. 2013.
[26] A. Godeke, "Performance Boundaries in Nb_3Sn Superconductors," University of Twente, 2005.
[27] J. Schindelin, I. Arganda-Carreras, E. Frise, V. Kaynig, M. Longair, T. Pietzsch, S. Preibisch, C. Rueden, S. Saalfeld, B. Schmid, J.-Y. Tinevez, D. J. White, V. Hartenstein, K. Eliceiri, P. Tomancak, and A. Cardona, "Fiji: an open-source platform for biological-image analysis," *Nat. Methods*, vol. 9, no. 7, pp. 676–682, Jul. 2012.
[28] Schneider C A, Rasband W S and Eliceiri K W, *ImageJ/FIJI 2012 NIH Image to ImageJ: 25 years of image analysis Nat Methods 9 671–5; Schindelin J, Arganda-Carreras I, Frise E, Kaynig V, Longair M, Pietzsch T, Preibisch S, Rueden C, Saalfeld S, Schmid B, Tinevez J-Y, White D J, Hartenstein V, Eliceiri K, Tomancak P and Cardona A 2012 Fiji: an open-source platform for biological-image analysis Nature Methods 9 676–82.* .
[29] D. S. Easton and D. M. Kroeger, "Kirkendall voids–A detriment to Nb_3Sn superconductors," *IEEE Trans. Magn.*, vol. 15, no. 1, pp. 178–181, Jan. 1979.
[30] L. Oberli, "Development of the Rutherford Cable for the EuCARD High Field Dipole Magnet FRESCA2," *IEEE Trans. Appl. Supercond.*, vol. 23, no. 3, pp. 4800704–4800704, Jun. 2013.
[31] C. Scheuerlein, M. Di Michiel, G. Arnau, R. Flukiger, F. Buta, I. Pong, L. Oberli, and L. Bottura, "Coarse Grain Formation and Phase Evolution During the Reaction of a High Sn Content Internal Tin Strand," *IEEE Trans. Appl. Supercond.*, vol. 21, no. 3, pp. 2554–2558, 2011.
[32] H. Veringa, P. Hoogendam, and A. Wees, "Growth kinetics and characterization of superconducting properties of multifilament materials made by the ECN powder method," *IEEE Trans. Magn.*, vol. 19, no. 3, pp. 773–776, May 1983.
[33] G. Roth and H. Krauth, "Reinforced superconductor element," US20090050348 A1, 26-Feb-2009.
[34] M. Brown, C. Tarantini, Starch, W., Oates, W., Lee, PJ, and Larbalestier, DC, "Correlation of filament distortion and RRR degradation in drawn and rolled PIT and RRP Nb_3Sn wires," 2016.